Title
Effect of Pore Pressure Oscillations on Fracture Permeability Enhancement

Author
Fakhartousi, Roohollah

Publication Date
2016

Peer reviewed|Thesis/dissertation

UNIVERSITY OF CALIFORNIA,
IRVINE

Effects of Pore Pressure Oscillation on Fracture Permeability Enhancement

THESIS

submitted in partial satisfaction of the requirements
for the degree of

MASTER OF SCIENCE

in Civil Engineering

by

Roohollah Fakhartousi

Thesis Committee:
Professor Russell Detwiler, Chair
Professor Soroosh Sorooshian
Professor Kuo-lin Hsu

2016

DEDICATION

I want to dedicate this work to my beloved parents. Without their support I could not have thrived at UCI. Special thanks also goes to my dear partner who made my life at UCI fun and joyful.

Last but not least, I am glad that I worked under the supervision of Professor Russell Detwiler, whose guidance directed me in every challenge that I faced during my research at the Subsurface Processes Lab. I also want to thank my thesis committee members, Professors Sorooshian and Vrugt. It was an honor to have them as my committee members.

TABLE OF CONTENTS

LIST OF FIGURES

LIST OF TABLES

ACKNOWLEDGMENTS

I thank everybody helped me to finish this work specially my lab mates at Subsurface Processes Lab, who helped me with my experiments and analyses.

ABSTRACT OF THE THESIS

Effects of Pore Pressure Oscillation on Fracture Permeability Enhancement

By

Roohollah Fakhartousi

Master of Science in Civil Engineering

University of California, Irvine, 2016

Professor Russell Detwiler, Chair

It is known that earthquake and seismic activities changes behavior of a hydrological system. These changes are attributed to changes in permeability of the medium due to pore pressure oscillations induced by seismic waves. Multiple studies suggest that fine particle mobilization inside fractures due to these oscillation, may be the possible mechanism that enhances permeability; however, direct evidence is lacking. Here I introduce a set of experiments to further analyze effects of pore pressure oscillations on fine particle mobilization inside a transparent analog fracture. I performed a controlled perturbation, using the designed oscillator, with peak flow rate of 1.9 ml/min and frequency of 1 Hz for 5 minutes. Effective aperture or hydraulic aperture is widely used in aperture studies to represent permeability of a fracture. In this study I observed that effective aperture enhanced by pore pressure oscillations from 58.77 μm to 73.23 μm. This enhancement was correlated to the particles that were mobilized during the oscillations. The particle mobilization was also visible in the animation created from the images that were taken during the experiment.

Chapter 1

Introduction

It is well documented that earthquake and seismic activities will change hydrological behavior of a system thousands of kilometers from the epicenter. Transient changes in water well levels [Coble, 1965, Roeloffs, 1998, Brodsky et al., 2003, Elkhoury et al., 2006], anomalous tidal responses [Manga and Wang, 2007, Xue et al., 2013], mud volcanoes and geysers [Manga, 2007], and anomalous stream and spring discharge [Manga et al., 2003, Manga and Rowland, 2009] all were detected surprisingly far from the causative earthquake. These changes last long after the earthquake and affect regions far from the main shock. Dynamic shaking also has been implemented for enhancing oil recovery in petroleum reservoirs, where fluid flow is enhanced by stimulating of the reservoir by low amplitude stresses. [Beresnev and Johnson, 1994, Kouznetsov et al., 1998]. Most authors suggest that these hydrological responses of the systems to seismic waves can best be described by permeability enhancement that is persistent after the passage of the seismic waves [Manga and Brodsky, 2006, Elkhoury et al., 2006, Liu and Manga, 2009, Elkhoury et al., 2011, Xue et al., 2013, Candela et al., 2014]. The dynamic strains of passing seismic waves produce pore pressure oscillations [Brodsky et al., 2003] and these oscillations enhance permeability in the fractured formation. Observations show that this response is transient and recovers to its initial condition long after occurrence

of the earthquake. Studies have observed permeability enhancement and its recovery to initial condition both in the field [Elkhoury et al., 2006] and laboratory [Elkhoury et al., 2011, Candela et al., 2014]. However, the mechanism by which this enhancement is induced is poorly understood. Three potential mechanisms have been suggested: (I) mechanical deformation of the fracture, (II) formation of micro-cracks and (III) clogging and unclogging of pore throats due to particle mobilization.

Faoro et al. [2012] suggested that deformation of fracture apertures due to pressure perturbation could be the possible explanation of the permeability enhancement. Pore pressure increases in fractures cause opening and subsequent permeability enhancement. Manga et al. [2012] observed formation of micro-cracks perpendicular to the fracture plane and considered the storage effect of these cracks as the possible mechanism that suggests recoverable permeability enhancement of the system. This mechanism does not actually enhance the permeability. The micro-cracks form with high peak in the pressure oscillation and fluids accumulates in them. When pressure subsequently decrease, these fluids flow back to the system causing enhanced fluid flow which may be misinterpreted as permeability enhancement. Mobilization of fine particles due to pore pressure oscillations has been the most supported possible mechanism for permeability enhancement. Liu and Manga [2009] suggested that particles trapped in pore throats and small pores, get mobilized by the dynamic stress induced by the oscillations. This unclogging of the throats, provides leads to larger paths for fluid flow and hence permeability is enhanced.

Elkhoury et al. [2011], Candela et al. [2014] developed an experimental procedure to examine both hydrological and mechanical responses to pore pressure oscillations. Their measurements of sample deformation show that the fracture opening was not enough to induce such an enhancement in the permeability. Microscopic observations and fluid chemistry test (described in next chapter) provide positive evidence of fine-particle mobilization. They attributed permeability enhancement and its slow recovery to the fine particle mobilization;

however, their experiments did not provide direct observations of this mechanism.

Although previous studies support the potential importance of fine-particle mobilization, the lack of direct quantitative measurements of the process motivates additional experiments. I have developed an experimental system capable of testing the hypothesis that "pore pressure oscillations mobilize trapped fine particles and enhance permeability; this enhancement is controlled by the amplitude and frequency of the oscillations". My experimental setting enables a real time visualization of the analog fracture and direct control of the oscillation parameters. Therefore, in this study we quantify the relationship between particle mobilization and permeability enhancement and examine the effects of oscillation characteristics on the enhancement.

Chapter 2

Background

In this chapter, I discuss previous studies in more details and define a set of focused research objectives in support of testing my hypothesis. Also I introduce different particle retention mechanisms inside fractures and discuss how they can be differentiated.

2.1 Fine Particle Mobilization As The Possible Mechanism

Elkhoury et al. [2011] performed a set of experiments to analyze effects of dynamic stress on permeability in fractured rock core samples. They artificially fractured a rock sample and induced a pore pressure oscillations to it. They were the first to capture permeability enhancement due to pore pressure oscillation at the lab scale. Their results can be summarized in Figure 2.1, which shows permeability along with inflow and outflow over the period of their experiment. Time zero is the start of the oscillations. This graph indicates a step increase in permeability right after the oscillations and it recovers to its initial value. Figure 2.1 (b) demonstrates the relationship between permeability increase normalized by

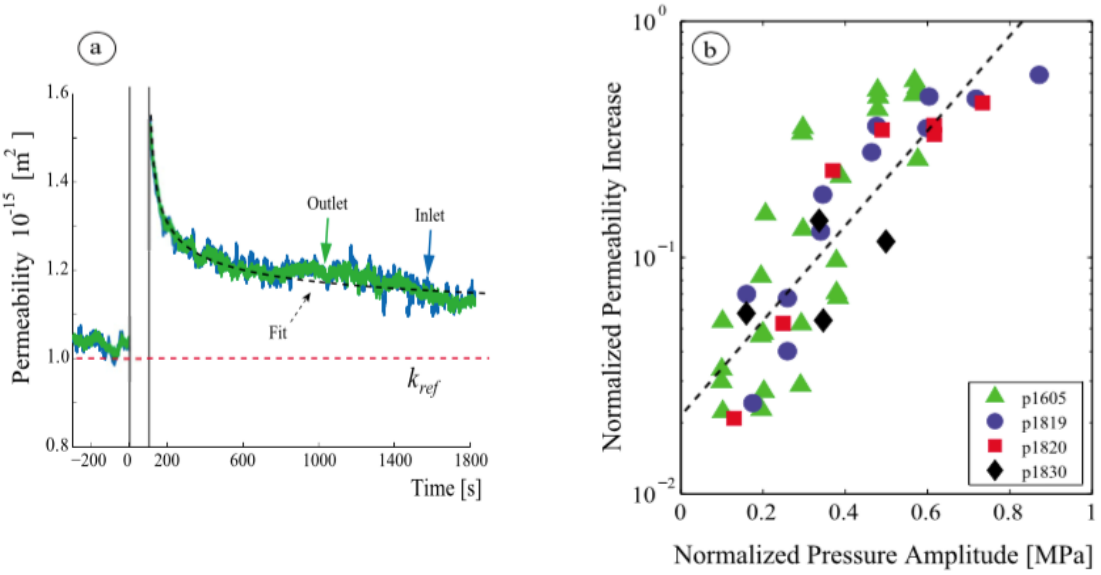

Figure 2.1: (a) Reproducing permeability enhancement by pore pressure oscillation in the lab. This graph shows a step increse in the permeability after oscillation followed by a gradual recovery. (b) Normalized permeability changes by K_{ref} versus normalized oscillation amplitude by differential pore pressure. This graph shows the direct relationship between permeability enhancement and the oscillation amplitude.

initial permeability and oscillation amplitude normalized by differential pore pressure. This graph indicates that the amount of permeability enhancement is directly proportional to the amplitude of the oscillation and it is dependent on the initial permeability value.

Based on indirect observations they postulated that mobilization of the fine particles is the possible reason for the permeability enhancement due to the oscillation. These observations were: (1) recovery of the initial permeability after dynamic stressing, (2) the dependence of the permeability enhancement on the initial permeability of the sample, (3) a lack of permeability increase for unfractured, intact samples, and (4) a lack of observed normal stress oscillations and displacements normal to the fracture plane. They all suggest that fine particle mobilization could be the possible mechanism for permeability enhancement but they lacked direct evidence. Hence, Candela et al. [2014] modified Elkhoury et al. [2011]'s

experiment to properly determine the mechanism by which the pore pressure oscillations induce permeability enhancement. They reproduced the former results, but also observed permeability enhancement in an intact (not fractured) sample. This is clearly in conflict with the results of Elkhoury et al. [2011], where they did not observe any enhancement in permeability in an intact sample.

In conjunction with reproduction of the experiments of Elkhoury et al. [2011], they added several new tests to examine different mechanisms of permeability enhancement. The first test was measuring the deformation normal to the sample to evaluate the importance of deformation mechanism on permeability enhancement. The measurement of sample deformation, via an internal LVDT, showed that dynamic stressing does not produce permanent deformation in fractured or intact samples. They calculated the fracture opening required for inducing the observed enhancement and they were two order of magnitude larger than what they observed. The result of this test rules out deformation of the fracture as the possible mechanism for the enhancement.

For the next test they took microscopic images of the fracture surfaces after the experiment and compared that to the images before the experiment. Post-experiment microstructural observations of the fracture surfaces reveal that most of the gouge was distributed in the downstream direction. The scanning of the sample before the experiment showed that most of the pores were filled by Kaolinite clay particles. Interestingly, after the experiments, the pore throats closer to the preferential flow path appear relatively clean while the farther pores were still occupied by the particles. These observations highlight the importance of particle mobilization but they are not direct evidences that pore pressure oscillation mobilizes the trapped particles; because the natural flow of fluid could flush out those clay particles and it does not clearly indicate pore pressure oscillations as the cause.

They also changed the fluid chemistry by adding different concentration of salts. They observed that changes in salt concentration had no effect on permeability enhancement for the

fractured sample. However, they noticed significant differences in the enhancement values for the intact sample. This observation again is not conclusive that the pore pressure oscillation mobilized the particles and enhanced the permeability. It certainly implies the importance of fine particles but there is no direct relationship between oscillations and particle mobilization. Also this test was only applicable for the intact sample and not the fractured samples. This is in contrast with Elkhoury et al. [2011]'s results, where they did not observe any enhancement for the intact sample.

The results and conclusions of the previous studies highlighted particle mobilization as the possible mechanism for permeability enhancement after the oscillations. This motivates further study of the mechanisms by which fine particles become trapped/released and the subsequent influence on permeability. In this study I built on prior work and developed a new suite of experiments to better understand the role of particle mobilization on permeability enhancement. My experimental set up allows me to directly visualize inside of the fracture during the experiment.

2.2 Particle Retention In The Fracture

Previous studies confirm the existence of fine particles in fractures and studied their transport through fractures. Various mechanisms affect particle transport and retention in porous media. Among these mechanisms straining (particles getting trapped at small pore throats) and physicochemical filtration (diffusion, interception and gravitational sedimentation) have more significant effects on particle deposition [Elimelech and O'Melia, 1990]. Reimus [1995] predicted an optimum particle size, greater than which would lead to particle retention due to gravitational settling or straining in small aperture regions of the fracture. Auset and Keller [2006] studied the importance of T/C (pore throat size to particle size ratio) when straining is the primary retention mechanism. They suggested for T/C less than 1.8, straining is

the primary retention mechansim. Becker et al. [1999] quantified the relative importance of gravitational sedimentation to diffusion by introducing settling and diffusion length scales. By implementing Stoke's velocity of settling he defined the settling length scale (L_s) as

$$L_s = (\frac{1}{18\mu})(\rho_p - \rho_f)gd_p 2\tau \tag{2.1}$$

and the diffusion length scale (L_D) as

$$L_D = \sqrt{2D\tau} \tag{2.2}$$

where the diffusivity, D is defined by

$$D = \frac{\kappa T}{3\pi\mu d} \tag{2.3}$$

where

d: particle diameter (cm)

ρ_p: particle density (g/cm^3)

ρ_f:fluid density(g/cm^3)

μ: dynamic viscosity ($g/cm.sec$)

g: gravitational acceleration (cm/s^2)

T: temperature (K)

κ: Boltzman constant ($1.4 \times 10^{-16}\ erg/K$)

τ: time interval (s)

The retention mechanisms and their effect on permeability decrease of the fracture were examined during the early developing stage of the experiment.

2.3 Clay Particles Characteristics

Clay particles are abundant in subsurface environments. They are colloidal particles that behave interestingly under different conditions. They generally carry negative charges which are neutralized by the presence of cations. Bentonite and kaolinite are two of important types of clay particles. Although they are similar in many properties, benotonite particles have swell in the presence of water while kaolinite particles do not undergo any expansion in water suspensions. Bentonite particles also tend to form a structure that causes the suspension of bentonite in water to form gel of relatively low concentrations. The inter-particle association is much stronger in bentonite suspension than kaolinite. [Luckham and Rossi, 1999].

The size of colloindal particles is generally less than about 2 to 5 μm. However, clay particles flocculate in water suspension and form aggregates with larger diameter. The clay type, salt concentration in the suspension and the valance of the cations are important factors determining size of the aggregates. Stawinski et al. [1990] found the mean diameter of these aggregates for 0.5 % concentration of bentonite and kaolinite in deionized water (DI water) and they were 60 and 10 μm respectively.

2.4 Objectives

In this study I present direct observations that prove pore pressure oscillations mobilize particles that would bot be mobilized by natural flow of water. Then I will show that this particle mobilization enhances the permeability. In summary the objectives are:

- Develop an experimental setting capable of inducing pore pressure oscillation into a fracture, with visualization of inside the fracture
- Indicate direct observations that emphasize importance of fine particle mobilization on

permeability enhancement

- Define a relationship between particles in the fracture and its permeability

Chapter 3

Experimental Methods

In this chapter, the details of the experimental setup and apparatus are given. Also the different stages of the experiment and the materials used are introduced.

3.1 Apparatus

My experimental setting has two main parts; the analog fracture and the oscillator, which are shown in Figure 3.1 and Figure 3.2 respectively. The fracture was constructed by placing a piece of rough-walled glass on top of a piece of flat glass with dimension of 6" $\times$ 6" (Figure 3.1). The space between the two glass plates simulates a rock fracture. The sides of the fracture were sealed by pressing seals to them. the seals are made of a piece of polycarbonate with an elastic gasket glued to it. On top of the glass plates frames were placed and the space between them was filled with pressurized air. I exerted 20 psi of pressure to ensure that changes in pore pressure during flow did not affect the fracture opening. Using transparent glass to build the fracture enables us to directly visualize flow phenomena in the fracture (a detailed construction procedure is provided by Detwiler et al. [1999]). The fracture was

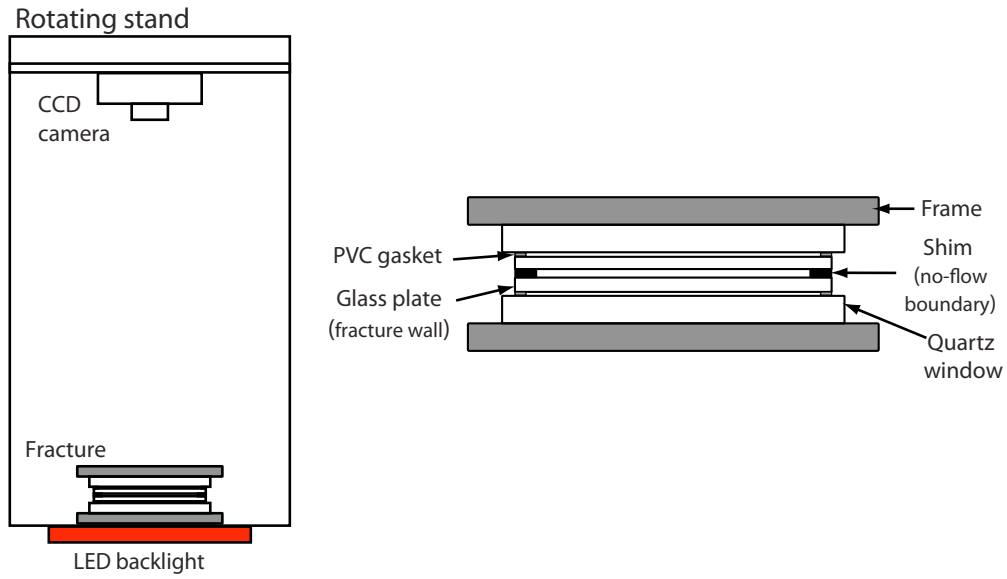

Figure 3.1: Analog fracture constructed by mating two pieces of glass each 6 inches. One is rough-walled and the other is flat

LED back-light panel on a rotatory stand. The light passes through the transparent fracture and is captured by the camera shown in Figure 3.1. The images taken by the camera are processed in MATLAB in order to quantify visualization of the fracture. I used light transmission techniques to visualize flow process inside the fracture. Schramm and Kwak [1982] developed a theory to determine clay concentration using light transmission through a suspension. They suggested that the number of particles per volume is directly related to the amount of light transmitted; however, their results were limited to very dilute suspensions and small particles. Here I ran a calibration experiment to determine a relationship between the light transmitted and the concentration. The results will be presented in the next chapter.

The oscillator was fabricated in a way to transmit the pore pressure oscillations to the flow system (Figure 3.2). There was no oscillator capable of generating pore pressure oscillations with frequencies in range of seismic waves and desired amplitude available in the Subsurface

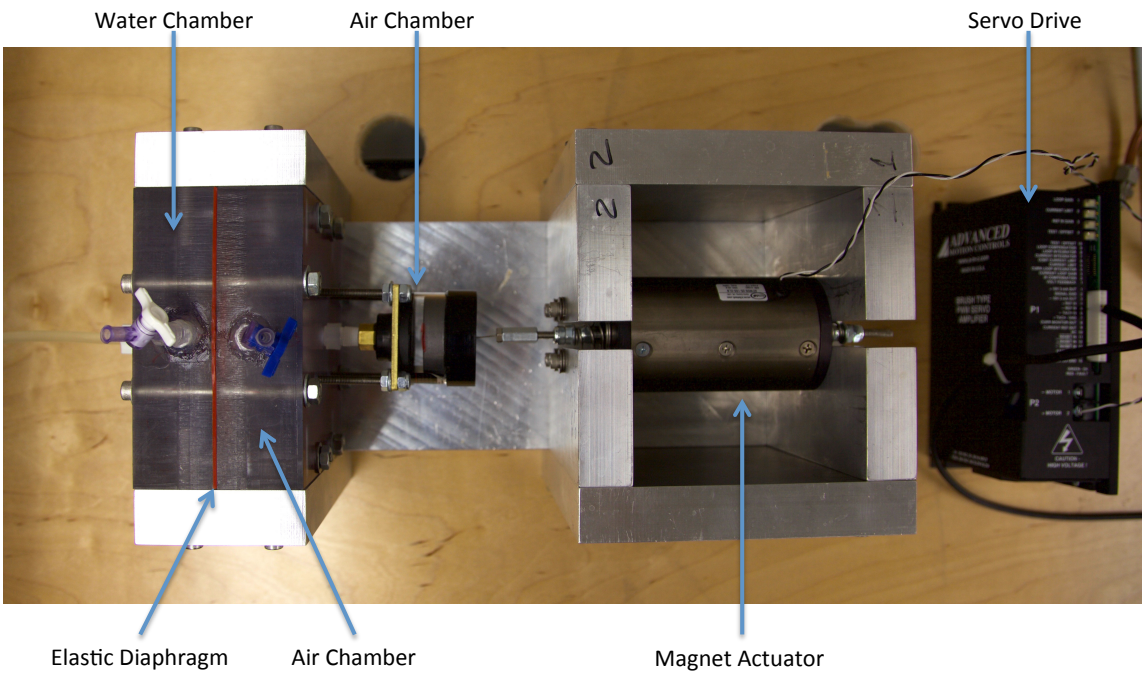

Figure 3.2: Oscillator

Processes Lab. Using AutoCAD and UCI campus machine shop, I designed and fabricated the oscillator device. The oscillator consists of a moving magnetic actuator, a piston, air chamber, elastic diaphragm and water chamber. The oscillation is generated by a moving magnet actuator (H2WTech, NCM08-25-100-2LB) which is controlled by a high switching frequency servo drive (Advanced Motion Controls, 16A20AC PWM). The servo drive is connected to an oscilloscope by which the oscillation amplitude and frequency are controlled. The moving part of the actuator is attached to a piston of an air cylinder which is connected to an air chamber. Another chamber, which is filled with water, is screwed to the air chamber with an elastic diaphragm in between to separate the air and water. The oscillation generated by the actuator is transmitted to the piston, the piston compresses/decompresses the air and the diaphragm transmits the oscillation to the water.

The peak flow rate of the oscillations generated by this fabricated oscillator were unknown. In order to exert a controlled perturbation into the system I ran a calibration experiment for

	Period (s)				
	10	8	5	3	1
Amplitude (Vpp)	Q (ml/min)				
1	0.2	0.3	0.4	0.6	0.4
2	0.6	0.8	1.0	1.2	1.2
3	1.0	1.2	1.5	1.7	1.6
4	1.3	1.5	1.8	2.2	1.7
5	1.5	1.8	2.1	2.6	1.9

Table 3.1: Results of calibration experiment for the oscillator

the oscillator. The experiment was aimed at quantifying the volume of water a designated oscillation can displace. A column of water in a graduated tube was attached to the oscillator. By generating different oscillations (different frequencies and amplitude) I measured the volume of water that was displaced by the correspondent wave. By dividing the volume over the period of the perturbation I calculated the peak flow rate that a particular input wave exerts on the system. Table 3.1 shows the calculated values for different waves and summarized in Figure 3.3.

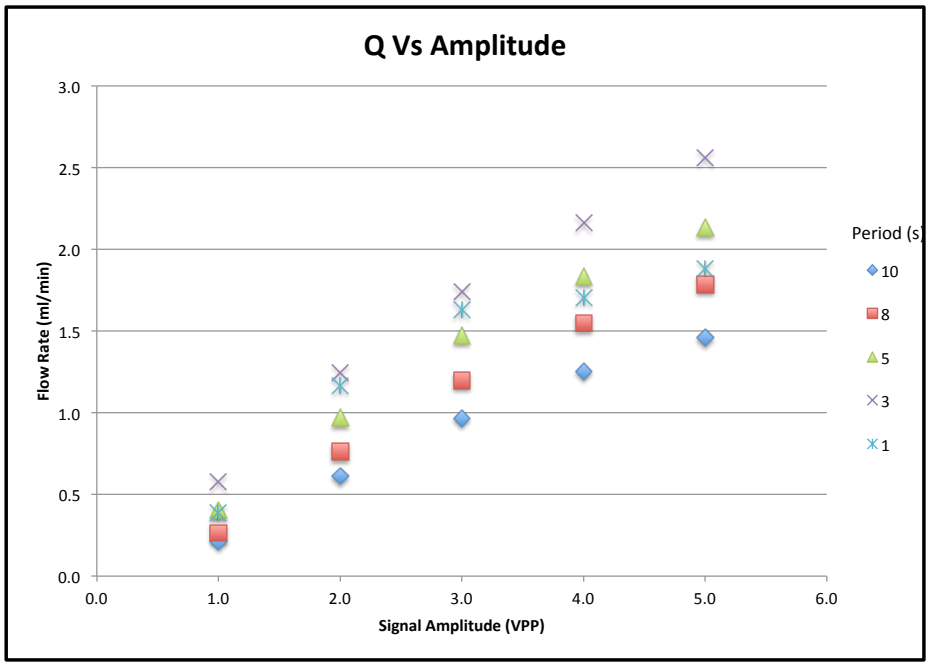

Figure 3.3: Oscillator calibration experiment. This graph shows flow rate Vs signal amplitude for a specific period.

3.2 Experiment Steps

The flow experiment was proceeded by different stages:

1. Measure the fracture aperture field
2. Initial waterflood to measure clean water permeability.
3. Injecting a suspension containing a known concentration of fines
4. Waterflooding and then measuring the reduced permeability due to particle retention.

5. Waterflood with oscillations.

6. Final waterflood and measuring the permeability after the oscillations.

During the entire experiment I measured flow rates and pressure differential at 60 seconds resolution to allow calculation of permeability over the time of the experiment.

To measure the fracture aperture field I followed the technique presented by Detwiler et al. [1999]. According to Beer-Lambert law:

$$I = I_0 e^{-\mu C b + \xi} \tag{3.1}$$

where

I: the transmitted light intensity,
I_0: the incident light
μ: absorptivity of the solute,
C: the solute concentration,
b: the gap width filled with absorbing solute and
ξ: a constant that accounts for absorbance by the solvent and the apparatus containing the solute [Detwiler et al., 1999]

By rearranging the equation for two solutions with different concentrations we set:

$$ln(\frac{I_1}{I_2}) = \mu(C_2 - C_1)b = A \tag{3.2}$$

where absorbance, A, of a solute is a linear function of concentration. To implement this equation I filled the fracture once with clear water and then by a solution of dye with known concentration. In each step I took images of the fracture to capture the light intensity profile. Therefore, A can be determined for the entire fracture by simply dividing the light intensity

profiles of clear water and dye solution. By considering C as the concentration of the dye

$$ln(\frac{I_{cl_{ij}}}{I_{dye_{ij}}}) = A_{ij} = \mu C b_{ij} \tag{3.3}$$

by averaging over the field

$$\langle ln(\frac{I_{cl_{ij}}}{I_{dye_{ij}}})\rangle = \langle A_{ij}\rangle = \mu C \langle b_{ij}\rangle \tag{3.4}$$

Combine equations 3.3 and 3.4 we have

$$\frac{b_{ij}}{\langle b_{ij}\rangle} = \frac{A_{ij}}{\langle A_{ij}\rangle} \tag{3.5}$$

Equation 3.5 suggests that if we know the mean aperture we can calculate the aperture field for the entire fracture. To measure the mean aperture I inject a known volume of water into the fracture and observed what area of the fracture was filled with that water (through image processing using MATLAB). Then the mean aperture is calculated by dividing the volume by the area that was filled with water.

Clear water permeability was measured using the Cubic law as the reference value for later comparison. In fracture studies, the Cubic law has been used for characterizing the flow through a fracture[Bear, 2013]:

$$Q = \frac{b_{eff}^3 g w}{12\nu}\frac{\Delta h}{l} \tag{3.6}$$

where

w: width of the fracture

ν: kinematic viscosity

l: length of the fracture

Δh: hydraulic gradient over the fracture

b_{eff}: effective aperture to the flow.

In this study I report the b_{eff} values as the reflective quantities for the permeability of the fracture, and I analyze the effects of particle retention and oscillations on the effective aperture. As seen in the equation, all other parameters are fluid dependent and effective aperture is the only representative of the medium. Witherspoon et al. [1980] introduced the following relationship between effective aperture and permeability for a fracture

$$k = \frac{b_{eff}^2}{12} \tag{3.7}$$

Therefore, this equation suggests that effective aperture is a meaningful representative of permeability for a fracture.

The procedure of measuring effective aperture is as follows. I injected water with various rates using the syringe pump. For each rate the corresponding Δh, pressure head difference along the fracture, was measured. Then a line was fit to the Q vs Δh data and effective aperture was calculated by the slope of that line. This procedure was repeated after the waterflooding and after the oscillation to measure the reduced and enhanced effective aperture respectively. Table 3.1 shows the flow rate and corresponding head difference for each stage of the experiment and in Figure 4.7 these data were plotted.

To create an initial condition for the fracture where there are fine particles distributed in the fracture, I start injecting the clay suspension prepared before. The particles are retained in the fracture and decrease the effective aperture. In preliminary experiments I used Sodium bentonite as the fine particles for the experiment. As I mentioned in chapter 2, bentonite particles tend to swell and form a gel-like fluid. This gel formation imposed some practical complexity and difficulties such as clogging the flow system or accumulation in flow manifolds so I used kaolinite particles, which did not show the same problems, for subsequent experiments. The $\%1 w/w$ suspension of kaolinite in DI water was prepared for

Q (ml/min)	h (cm) Clear Water	h (cm) After Clay Injection	h (cm) After Oscillation
0.25	0.86	2.55	1.36
0.50	1.67	5.10	2.69
0.75	2.51	7.62	4.01
1.00	3.34	10.13	5.34
1.50	4.98	15.24	7.99
2.00	6.64	20.29	10.59
2.50	8.30	25.28	13.15
3.00	9.94	30.09	15.56

Table 3.2: Head and flow rate data for different stages of effective aperture measurement.In all of these measurement water was injected with the given flow rates and correspondent head difference was measured for each experiment.

the clay injection process. Then the suspension was injected to the fracture with constant head. To provide a constant at the inlet, I used a Marriott's bottle to inject the clay suspension. A Marriott bottle is a device that delivers a constant head of flow from closed bottles or tanks. The injection process was stopped when the outflow reached a constant rate, which indicated a steady state condition for particle retention. No further particle retention and subsequent permeability reduction was observed after this point.

At this point I started injecting water to the system to flush out the particles that are not trapped in the fracture. I used a syringe pump to inject DeIonized-DeAired water with constant flow rate of 3 ml/min to the system and monitored the differential pressure across the fracture. I made sure that during the entire experiment, especially during the oscillations, the flow rate in the system did not exceed this value of 3 ml/min to ensure that particles that remained in the fracture are not mobilized due to excessive velocities. After reaching a steady state condition (constant differential head), I was certain that the remaining particles were trapped and cannot be mobilized by steady flow. The fracture after this stage provided the initial condition for the oscillations. The effective aperture was measured again to determine its value before the onset of pressure oscillations. This value is referred as after-flooding aperture.

At this time the fracture is ready to perform the oscillations. The oscillator was used to induce a controlled perturbation to the system. A sinusoidal wave with frequency of 1 Hz and amplitude of 4 Vpp was imposed on the flow system by the oscillator for 5 minutes. The calibration experiment confirmed that the peak flow rate produced by this wave is 1.9 ml/min. The syringe pump was set to the flow rate of 1 ml/min and injected water constantly to the system as the background flow for the oscillations process. In this way I was certain that the maximum flow rate was 2.9 ml/min, which is less than the waterflooding limit of 3 ml/min. In other words, I ensured that the differential pressure head perturbation is in range of the normal differential pressure head during waterflooding. After the oscillations the effective aperture was measured again to quantify the permeability enhancement and is called after-oscillation aperture.

All the experimental steps can be summarized in the Figure 3.4

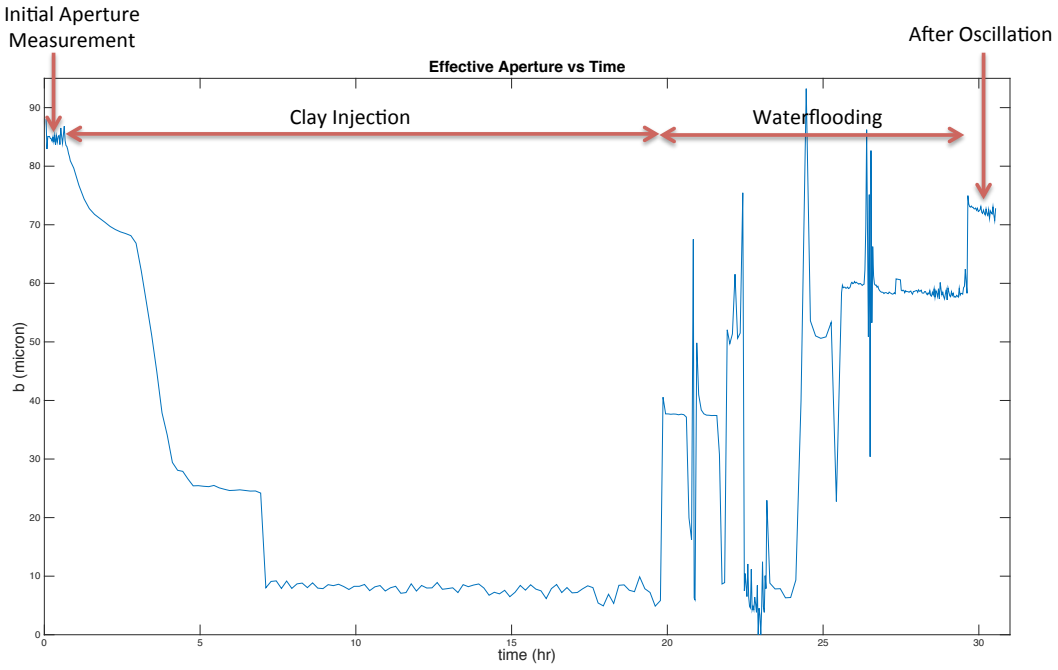

Figure 3.4: Effective aperture vs time. This figure shows major processes during experiment. Initial Aperture Measurement, Clay injection, Waterflooding & After Flooding Aperture Measurement and Oscillations.

Chapter 4

Results and Discussion

4.1 Light Transmission Calibration

In colloidal studies, most authors applied light scattering technique to evaluate the concentration of a colloid suspension. There has been no direct implementation of light transmission technique for estimating the high concentrated suspension to my knowledge. To assess the feasibility of measuring high concentration I ran a calibration experiment to relate the amount of light transmitted to the concentration. Nine different bentonite suspension with different concentrations ranging from $\%0.162 w/w$ to $\%2 w/w$ were prepared and correspondent absorbances were measured. The data points are shown in Figure 4.1. I fitted an empirical curve to the data points that best represents them. The equation for the fitted curve is:

$$A = \frac{aC^2 + bC + d}{C + e} \tag{4.1}$$

where $a = -0.474$,$b = 4.551$,$d = 0.00240$ and $e = 1.372$.

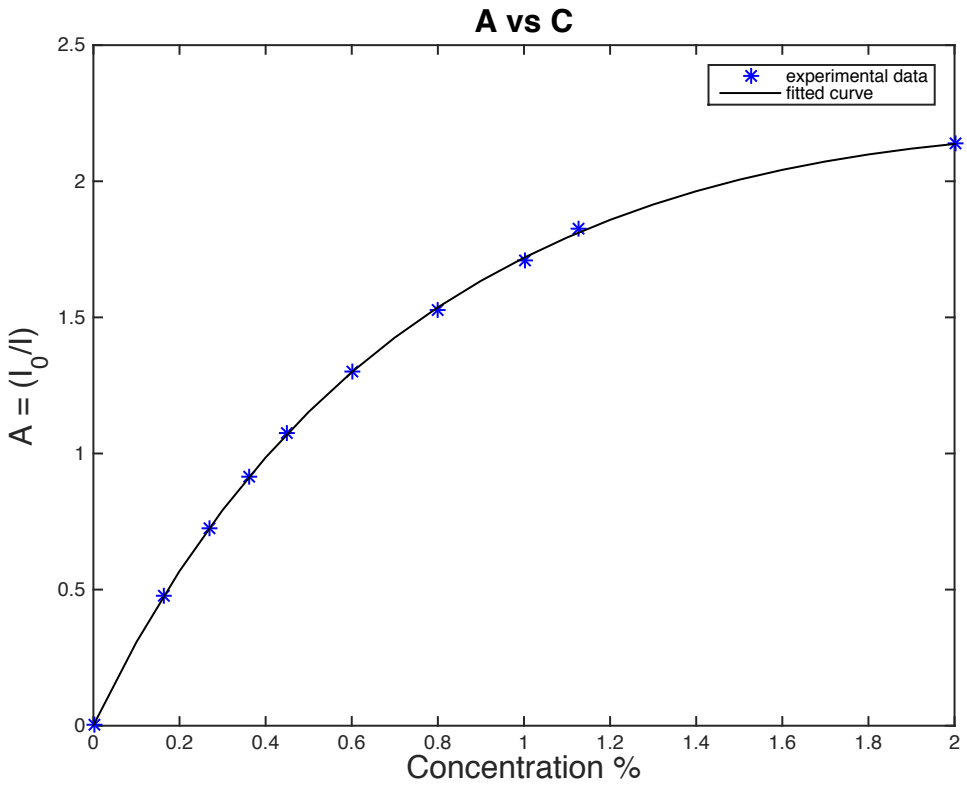

Figure 4.1: Plot of different concentration versus absorbance

This equation is applicable to bentonite concentration within the fracture. however as I mentioned in previous chapter, kaolinite particles were used in the main experiment due to challenges caused by gel formation with bentonite. Kaolinite particles are smaller than bentonite particles and do not endure gelation and swelling. Therefore they comply better with light transmission technique. Schramm and Kwak [1982] suggested a direct linear relationship between absorbance of the light transmitted and concentration of the suspension. I evaluated this hypothesis by testing the applicability of Beer-Lambert law to the experiment. According to this law, absorbance, A, should have a linear relationship with aperture, b, with a constant of μC, for a uniform concentration field. To attain this relationship, I plotted a 2D histogram of A vs b for the early stage of clay injection, when it is filled with one percent suspension of kaolinite. Figure 4.2 shows this plot.

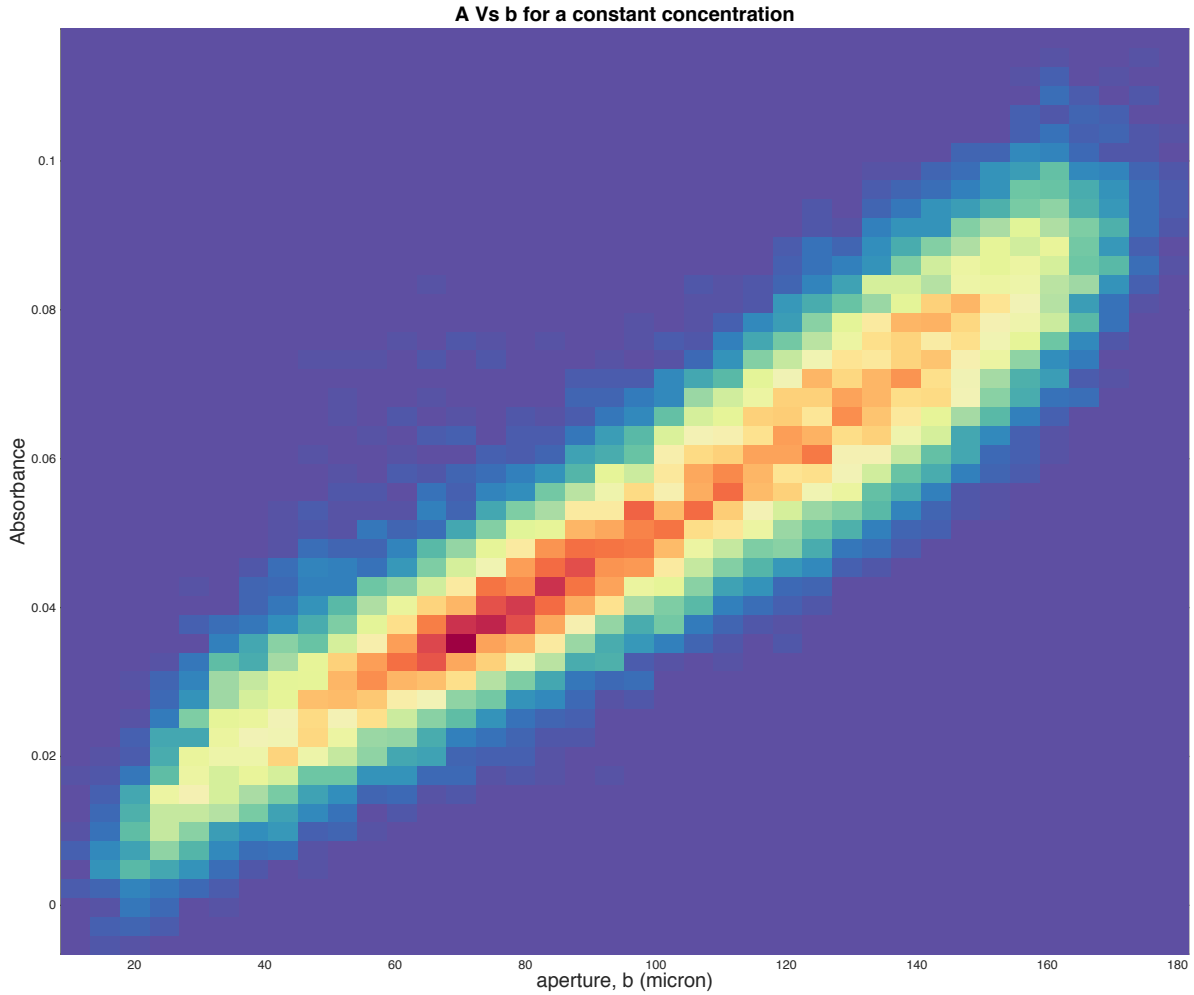

Figure 4.2: Absorbance versus aperture. This graph shows the linear relationship between A and b which supports the applicability of the Beer-Lambert law to the kaolinite suspension. The color scale implies frequency of a specific aperture and A.

Compliance of kaolinite suspension with the Beer-Lambert law suggests that there is a linear relationship between A and concentration, C. Hence, by having two points of this line, the relationship between A and C can be determined. As expected, this line intersects the origin because A must equal zero at zero concentration. The other point of this line was found by averaging the A for the entire fracture when it is fully saturated with one percent suspension.

For C = 1, the mean of A over the entire fracture, $A = 0.0519$. Therefore, the relationship between C and A established as:

$$C = 19.27A \tag{4.2}$$

4.2 Aperture Field and Particle Retention Mechanisms

The mean aperture was measured, to be 85.12 μm. The aperture field and its histogram is shown in Figure 4.3, with aperture ranging from 7 to 215 μm. The particle size according to the manufacturer data sheet was between 2.5 to 4 μm. However, clay particles tend to flocculate when they are in suspension and form larger aggregates [Luckham and Rossi, 1999]. Stawinski et al. [1990] found the flocculates mean diameter for $\%0.5w/w$ of kaolinite suspension with different salt concentrations. They reported the mean diameter of 10 μm for the suspension of kaolinite in DeIonized-water (DI water). Therefore, I considered 10 μm as the mean diameter for the particle size.

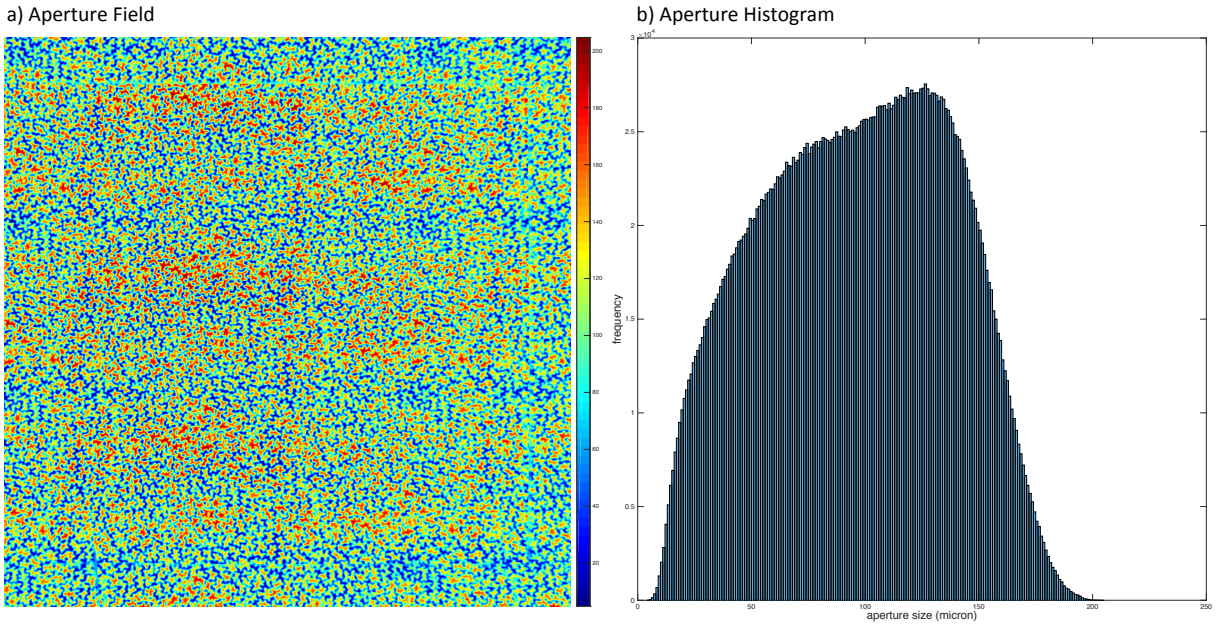

Figure 4.3: a) Apertue field of the fracture; b) Aperture field histogram

As I discussed before, for straining to be the retention mechanism the T/C ratio should be less than 1.8. Figure 4.4 a, shows the T/C ratio over the fracture area. The yellow areas are the regions with T/C less than 1.8, which indicates apertures with dominant straining. This image demonstrates that straining happens in small regions over the whole fracture and only 9.62 percent of the fracture is retaining the particles by straining. However, we will observe qualitatively that it has significant effect on effective aperture. This indicates that straining is

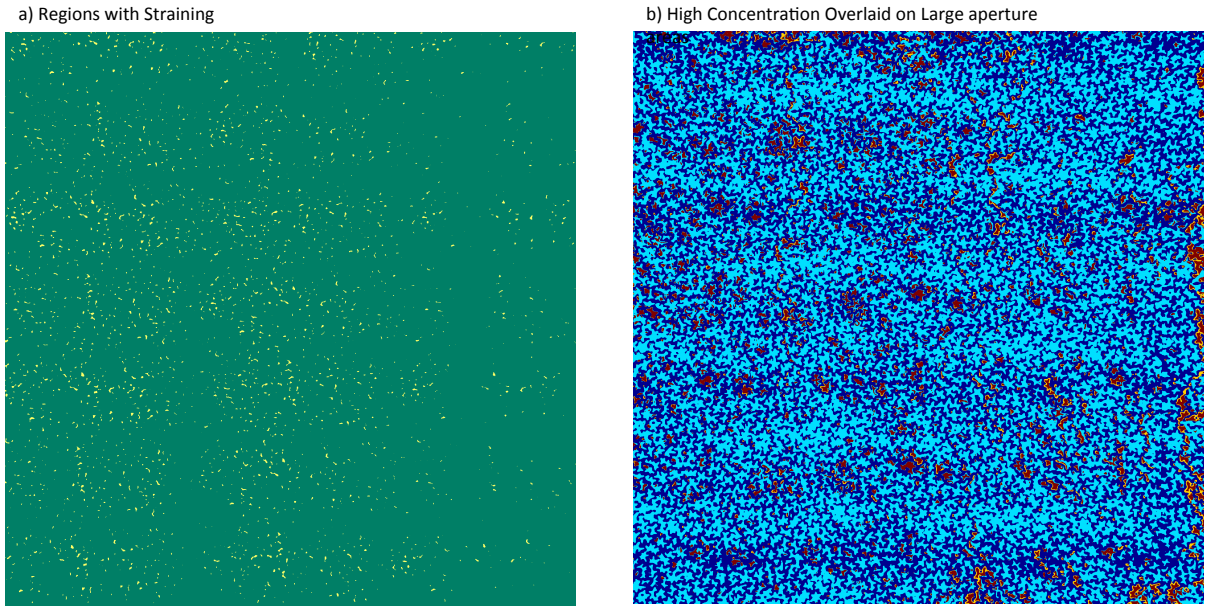

Figure 4.4: a) Straining analyzed by T/C ratio over the fracture; yellow areas indicate regions with T/C of less than 1.8 and high straining. b) Sedimentation; high concentrated regions showed as a layer on top of large aperture areas. The light and dark blue areas represent the large and small aperture regions respectively, the orange ones are regions with high concentration and the red regions are where high concentration of particles accumulated in large aperture regions. This figure indicates the importance of sedimentation compare to straining.

not the dominant retention mechanism and suggests that one of the physiochemical filtration mechanisms is controlling particle retention inside the fracture. Among them, interception is less likely to happen because clearly, there is no obstruction for the particles inside the fracture for interception to occur. In order to compare effects of diffusion and sedimentation, we implemented the approach of Becker et al. [1999]. For my experiment L_s and L_D were found to be 94 and 0.0001, respectively. This suggests that sedimentation is significantly more efficient than diffusion. Therefore gravitational sedimentation is the primary mechanism that

retains the particles in the fracture. This is supported by image processing results, which show that particles mainly accumulated in large aperture regions. Figure 4.4 b, shows the location of high concentration regions overlaid with aperture regions larger than the mean aperture, 85.12 μm. The light and dark blue areas represent the large and small aperture regions respectively, the orange ones are regions with high concentrations and the red regions are where high concentration of particles accumulated in large aperture regions. This figure shows that most of the particles settled in the large aperture regions and highlights the importance of sedimentation in particle retention inside this fracture.

4.3 Effective Aperture

Figure 4.5 shows flow rate and pressure head difference during the experiment. By applying the Cubic law to the flow rates and head data, I calculated the effective aperture over the entire experiment with a temporal resolution of 5 minutes (Figure 4.6). Effective apertures presented in this study are calculated with two different methods. In Figure 4.6 I averaged each 10 flow rates and head data and calculated each effective aperture based on the moving average. To attain more accurate values for effective aperture before and after the oscillations 3 different aperture measurement experiments were done. During these experiments I assumed that steady state condition for aperture were reached and the value was stable. Then I flowed water at 8 different flow rates and collected the correspondent head data. These experiments are denoted as 1) initial aperture, 2) after waterflooding and before the oscillation process and 3) after oscillation in Figure 4.5 b.

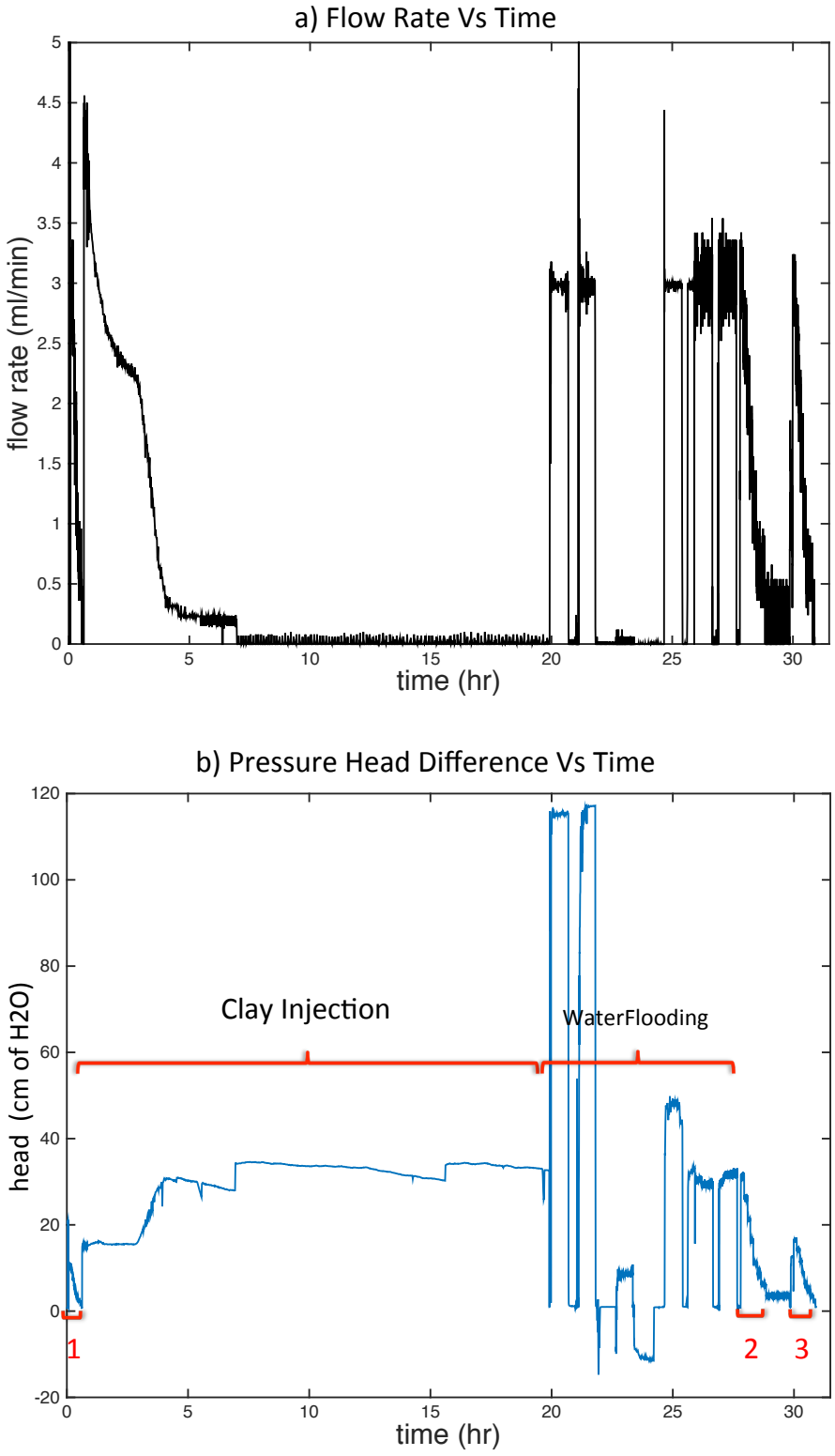

Figure 4.5: a) Flow rate Vs time during the experiment; b)pressure head difference along the fracture Vs time during the experiment.

Clear Water Aperture	After Flooding	After Oscillation Aperture
85.3 μm	58.77 μm	73.23 μm

Table 4.1: Calculated effective apertures for different stages of the experiment.

Figure 4.7 shows these three experiments separately. Table 4.1 summarizes the effective aperture values for different stages of the experiment calculated from data of Table 3.1 and Figure 4.7. According to Table 4.1 effective aperture is 85.30 μm for clear water, which was close the the measured mean aperture by Beer-Lambert's law, and drops to 58.77 μm when particles were retained in the fracture and eventually enhances to 73.23 μm after the oscillations.

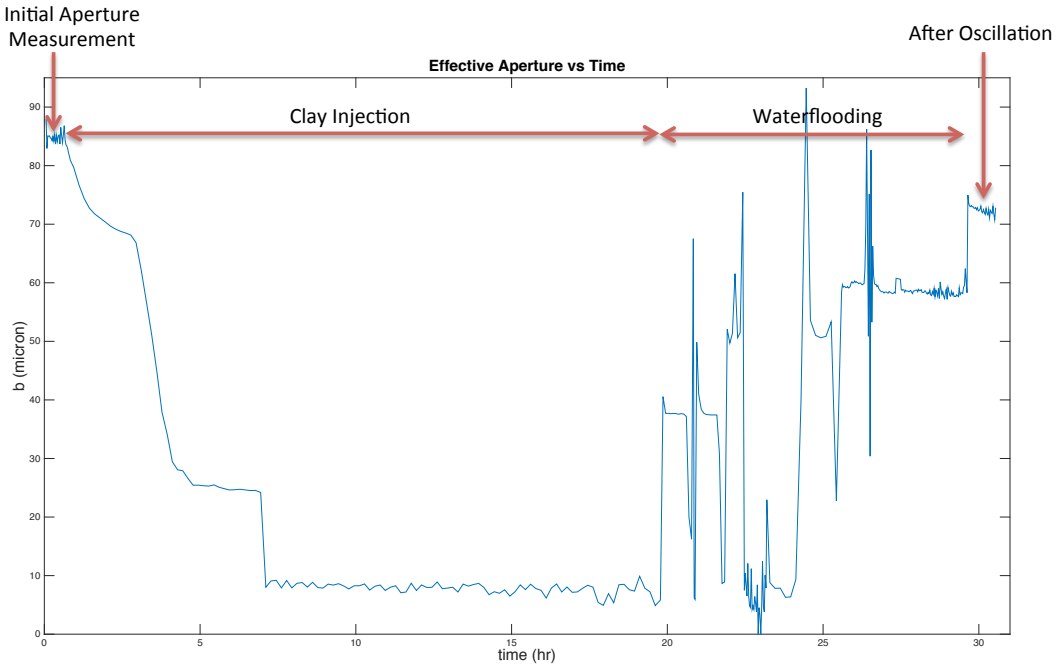

Figure 4.6: Effective aperture vs time. This figure presents effective aperture values during the entire experiment. An initial decrease due to particle retention, waterflooding and reaching to a constant reduced aperture value and finally a step increase on aperture due to pore pressure oscillations.

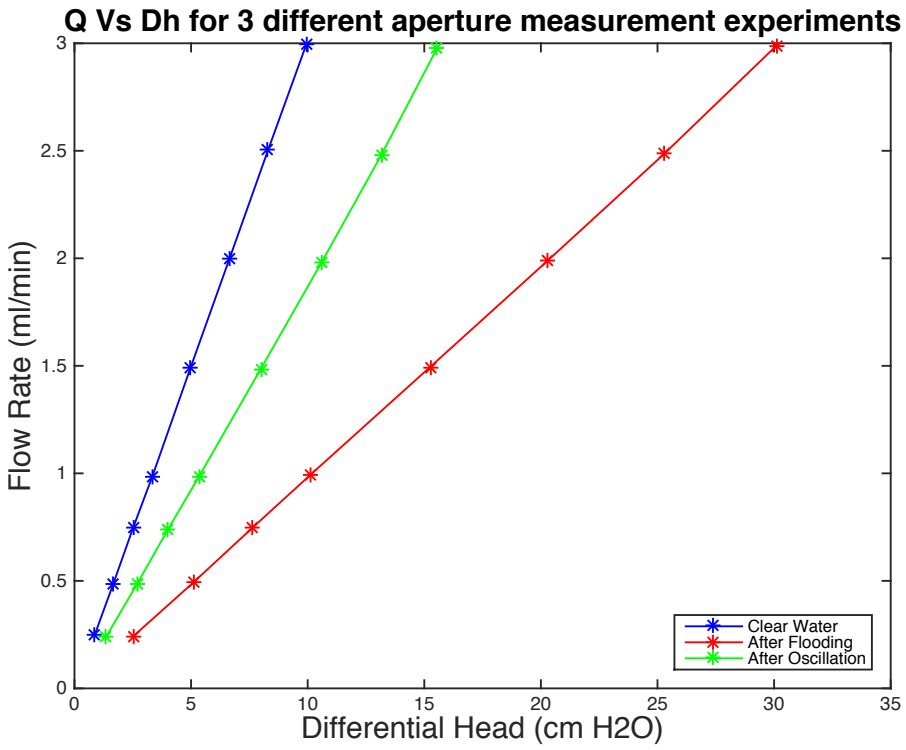

Figure 4.7: Flow rate Vs differential head along the fracture for 3 different aperture measurement experiments. They are denoted as 1) initial aperture, 2) after waterflooding and before oscillation process and 3) after oscillation in Figure 4.5 b.

When the clay injection process began, the effective aperture began decreasing from its initial value and eventually reached a constant value. As time elapses, more particles become stuck inside the fracture and the effective aperture decreases. Figure 4.6 suggests that the effective aperture experiences a sudden plunge in its value. This can be seen and explained by looking at the flow rate and pressure data during the clay injection process, Figure 4.8. As I mentioned in the previous chapter, I implemented a Marriott bottle to inject the clay suspension with constant differential head. However, the transducers are placed right before and after the fracture. Therefore, Figure 4.8 reflects the differential head along the fracture and not the entire system. In fact the flow system consists of all the tubings, fittings, manifolds and fracture.

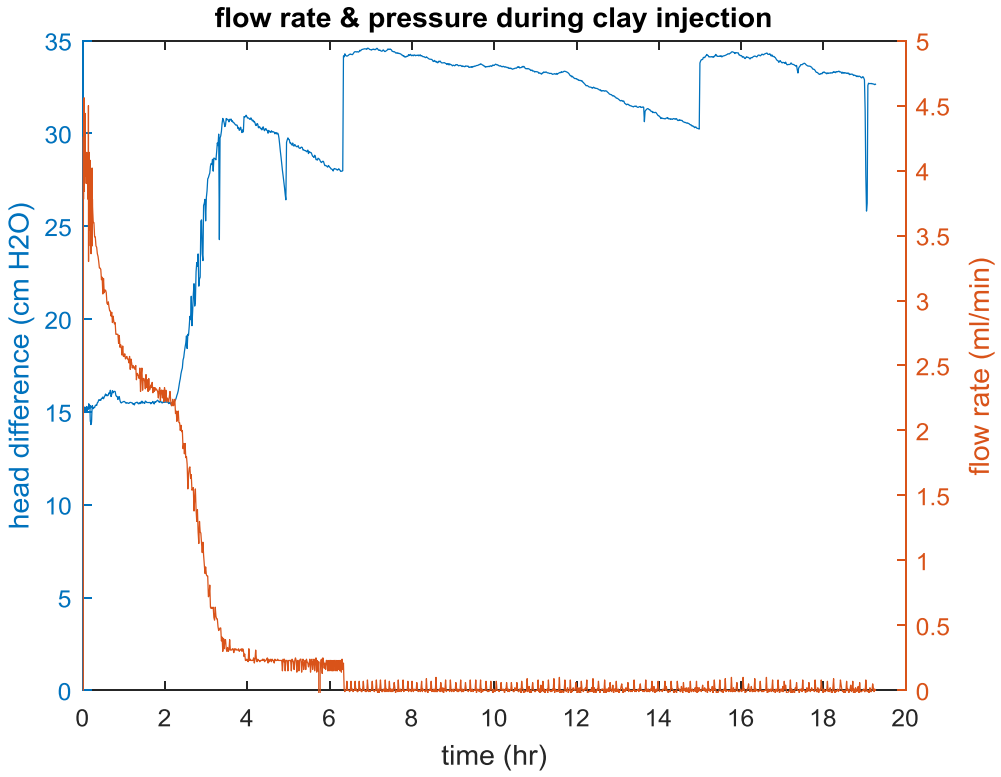

Figure 4.8: Flow rate and head data during the clay injection process. The fracture and the head data are best depicted in the animation created by the data and accessible through `https://www.youtube.com/watch?v=cKvFTQm-Bx0&feature=youtu.be`

Hence, the total head difference along the system is

$$h_t = h_{loss} + h_f \tag{4.3}$$

where h_t is total head and h_f is head loss along the fracture, which was measured by the transducers. For h_{loss}, head loss in the tubing, Darcy-Weisbach equation suggests

$$h_{loss} = \frac{128\nu L}{\pi g D^4} \tag{4.4}$$

for laminar flow where L and D are tubing length, 300 cm, and diameter, 0.15785, respec-

tively. The Marriott bottle was tested and confirmed that h_t was constant of 34 cm of H_2O for the system. The h_f values also were measured by the transducers along the fracture. The Reynolds number also was calculated by measured flow rate data and indicate laminar flow in tubing. Then I calculated the h_{loss} by Equation 4.4. I expected that sum of calculated h_{loss} and h_f would be equal to the 34 cm for the entire experiment. However, it was not the case. The reason for this strange behavior can be best explained by accumulation of particles in the tubing resulting in a reduction of the effective tubing diameter over time. This was actually observed during the experiment that particles tend to settle and accumulate inside the tubing and subsequently decrease the effective diameter for the flow. By applying Equation 4.4 as well as the flow rate and h_f data, I managed to calculate the effective diameter during the clay injection process and it is shown in Figure 4.9. The sudden increase around t = 15 hr is because the tubing was agitated to induce more

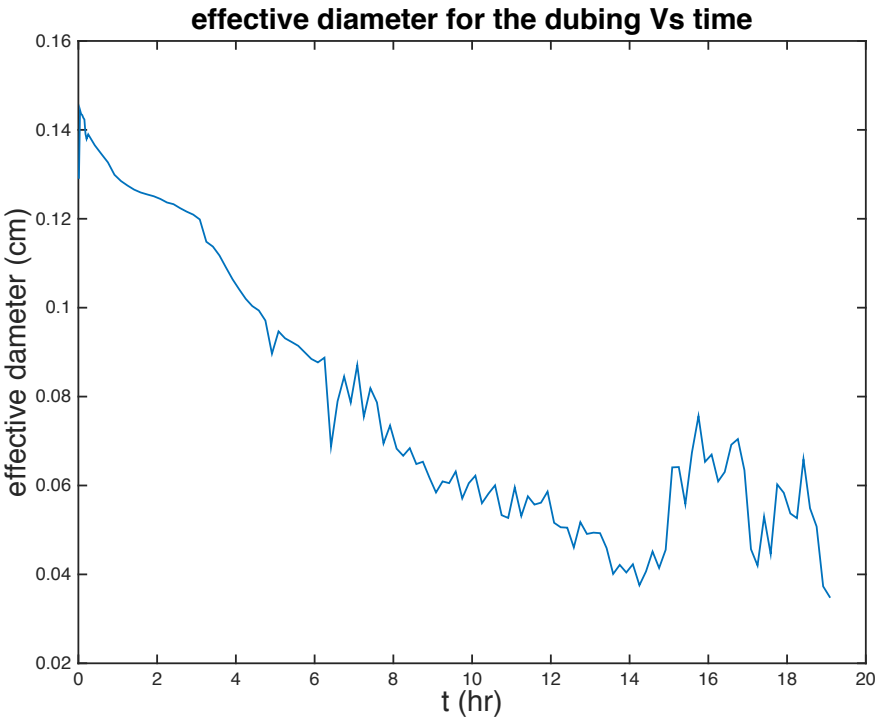

Figure 4.9: Effective diameter for the tubing. During clay injection process, particles sediment inside the tubing and that causes the effective diameter in head loss equation to decrease.

flow into the system and therefore some of the particles were released from the tubing enhancing the effective diameter.

By considering these new values for D in Equation 4.4, the new head loss was measured and then summed with the head difference along the fracture. Figure 4.10 shows this data for the clay injection period.

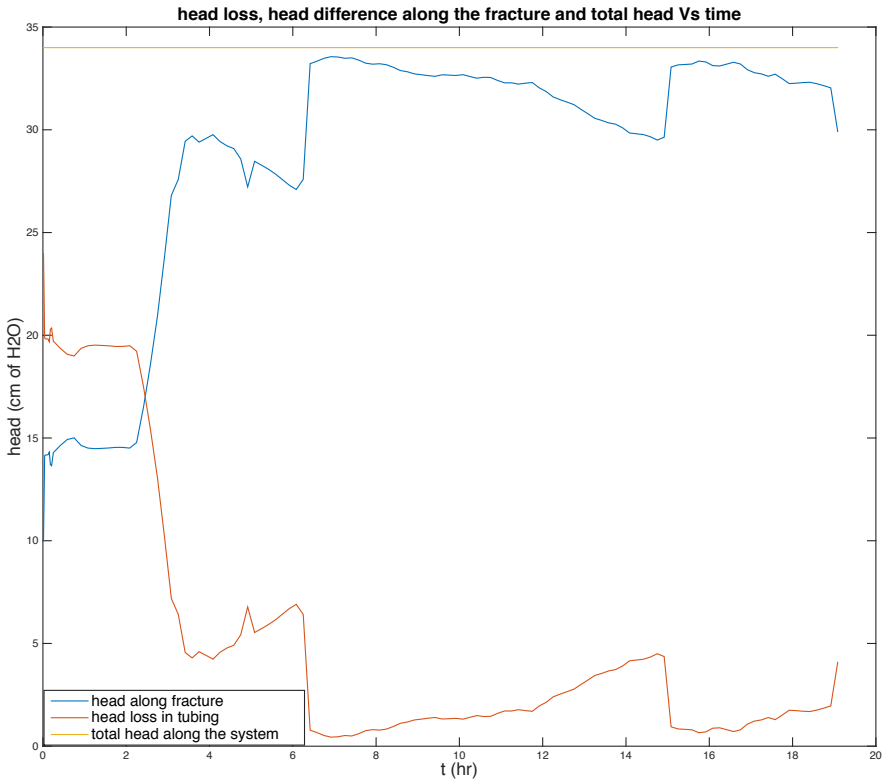

Figure 4.10: Head loss in tubing, head difference along the fracture and total head for the system.

After almost 6 hours of clay injection, the flow rate decreases to 0.07 and stays constant for 13 hours. This indicates that the flow process reached a steady state condition and particle retention is at equilibrium. It is also apparent in Figure 4.6 which shows a constant value of 10 μm for the effective aperture during this period.

After the steady state condition was confirmed, I started injecting water to flush out particles that are not trapped in the fracture. Because the capacity of the pump I used for waterflooding was very limited I had to stop and refill the syringes frequently. On the other hand, the settled particles in the inlet tubing and manifold clogged the path and resisted flow. These two processes distorted the data during the waterflooding process. Throughout this waterflloding process the flow rate was set at 3 ml/min on the syringe pump. Figure 4.5

shows the head data during the entire experiment and it indicates anomalous data during the waterflooding period. Due to resistance of flow caused by the settled particles in the manifold and tubing, the head increased to 117 cm of H_2O. In the course of waterflooding, negative head pressure is also observable. This is because sedimentation in the inlet tubing and manifold clogged the flow path completely so I back flowed to unclog the system. After 7 hours of waterflooding, the flow reached a steady state condition with a constant head of 30 cm of H_2O. To summarize the clay injection and waterflooding process, the effective aperture started decreasing when clay injection began, from 85.3 μm to 10 μm; then waterflooding flushed away some of the particles that were not trapped and increased the aperture to 58.77, Figure 4.6.

I induced pressure perturbation with amplitude of 4 Vpp and frequency of 1 Hz to exert a maximum of 2 ml/min of extra flow rate into the system. I did not collect head data during the oscillation because the frequency of the wave was higher than the acquisition rate of the transducer. After oscillation, the effective aperture increased to 75 μm and decreased, as flow continued, to 70 μm. I believe that pore pressure oscillations enhanced the effective aperture, which can be seen by the sudden jump in aperture value right after the oscillation. When oscillations stopped, particles tend to re-clog the throats and decrease the effective aperture.

Figure 4.11 shows the fracture sequentially throughout the entire experiment. As I started injecting clay particles they start to accumulate inside the fracture and decrease the effective aperture. The maximum amount of particles is in the fracture after the clay injection ended. By starting waterflooding some of the particles flushed out of the system and less particles remain in the fracture. I observed in the collected data that pore pressure oscillation mobilized the particles and that enhanced the effective aperture. Figure 4.12 shows the concentration profile inside the fracture right before, and after the oscillation along with their difference. It can be seen that after the oscillation stopped some of the particles were

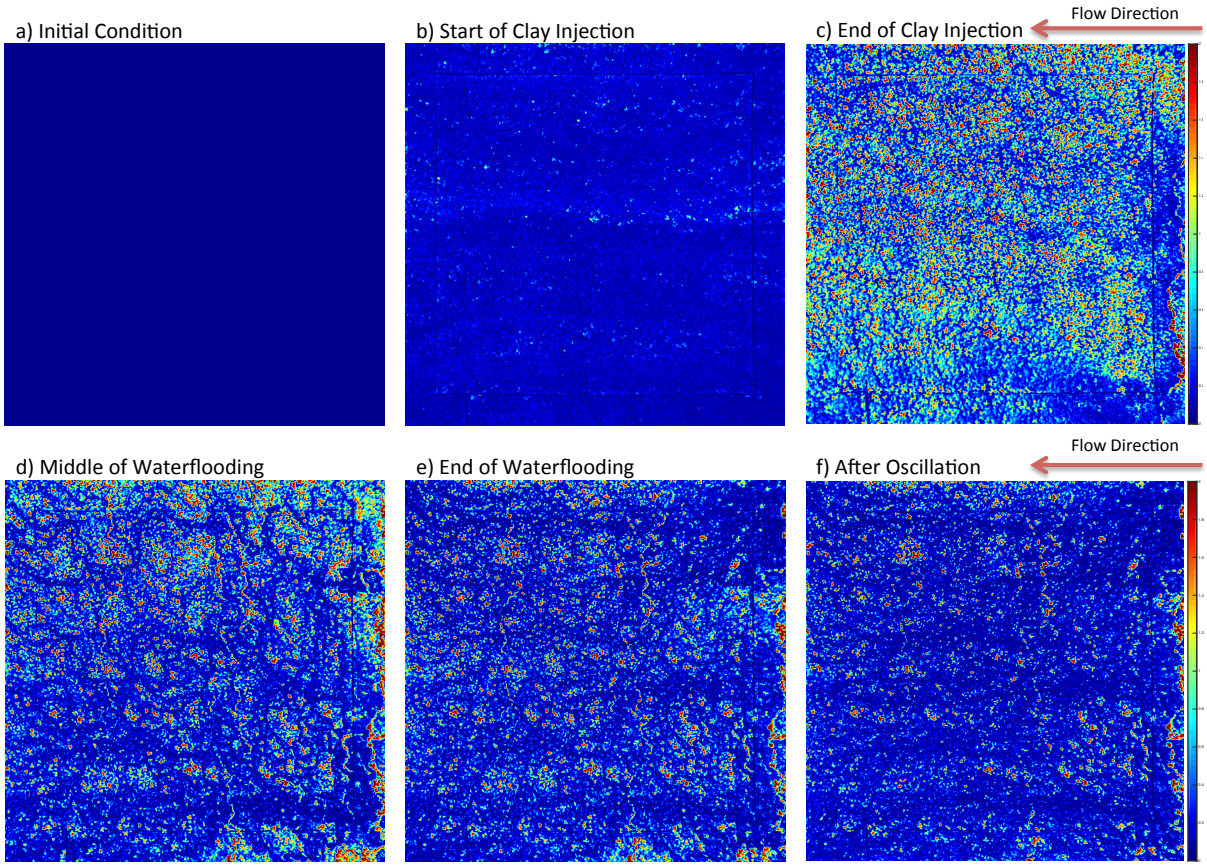

Figure 4.11: Images of fracture during different stages of the experiment. The color bar signifies the absorbance field inside the fracture ranging from red, high absorbance (high concentration) to blue, low absorbance (low concentration).

flushed out from the system, which is the cause for the permeability enhancement right after the oscillation. The difference between the two images demonstrates the amount of particles that were mobilized after the oscillation.

To determine better where the particles got mobilized from, I overlaid the high concentration regions in Figure 4.12 c, with large aperture regions and the straining dominant areas. Figure 4.13 shows these three quantities in the same image. The black and red regions represent small and large apertures, respectively. The orange shows high concentration regions and yellow indicates where the high concentration of particles were mobilized from large aperture. The white areas also show regions with dominant straining. I observed that effective aperture during oscillations increased by 14.46 μm and attributed this enhancement to par-

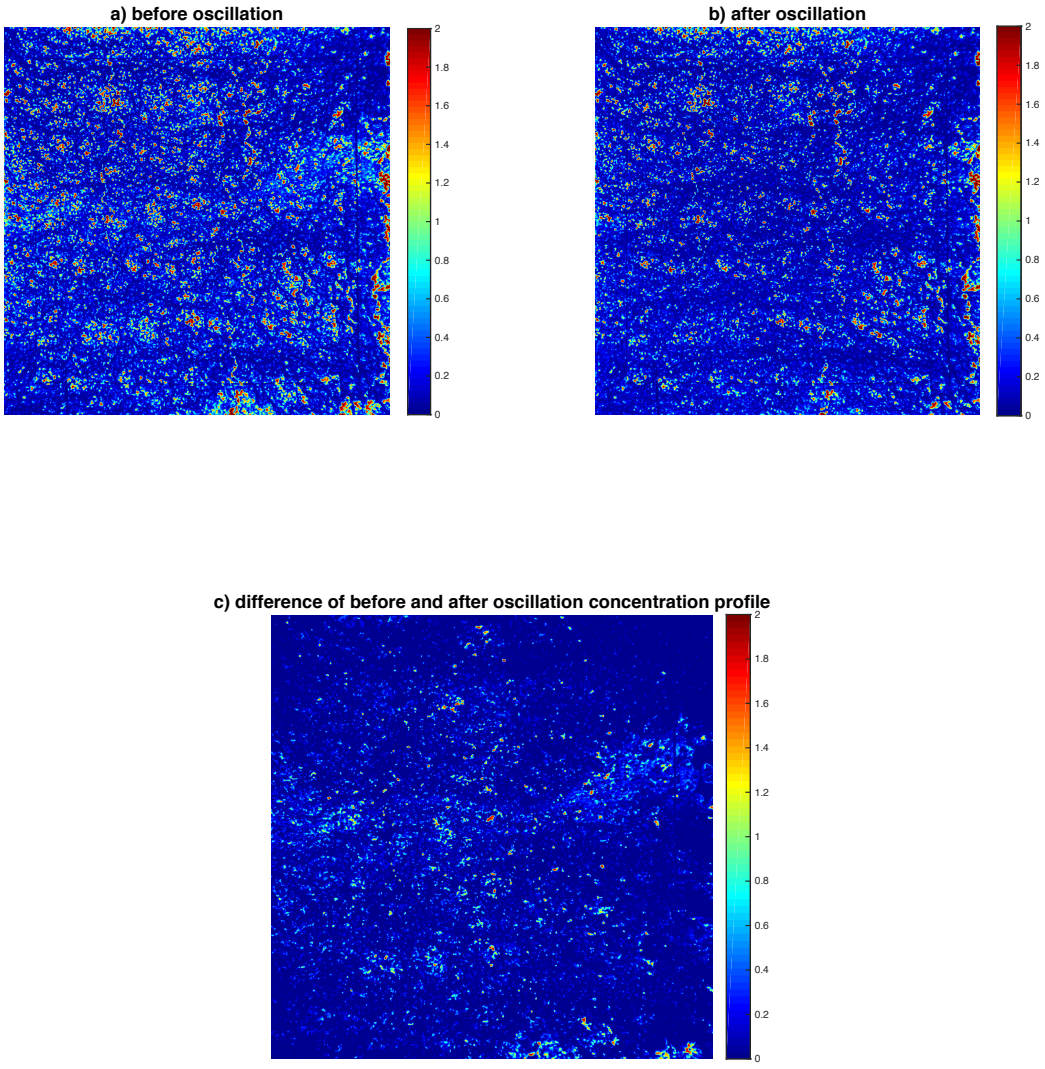

Figure 4.12: Concentration profile right a) before and b) after the oscillation. c) The difference between these two pictures which is evident of particle mobilization due to oscillation.

ticle mobilization. By looking at Figure 4.13, it can be seen that most of the particles were mobilized in large aperture regions but they were surrounded by small aperture and straining dominant regions. This suggest that although the primary particle retention mechanism is sedimentation, straining is more influential on effective aperture. I used this result in next chapter.

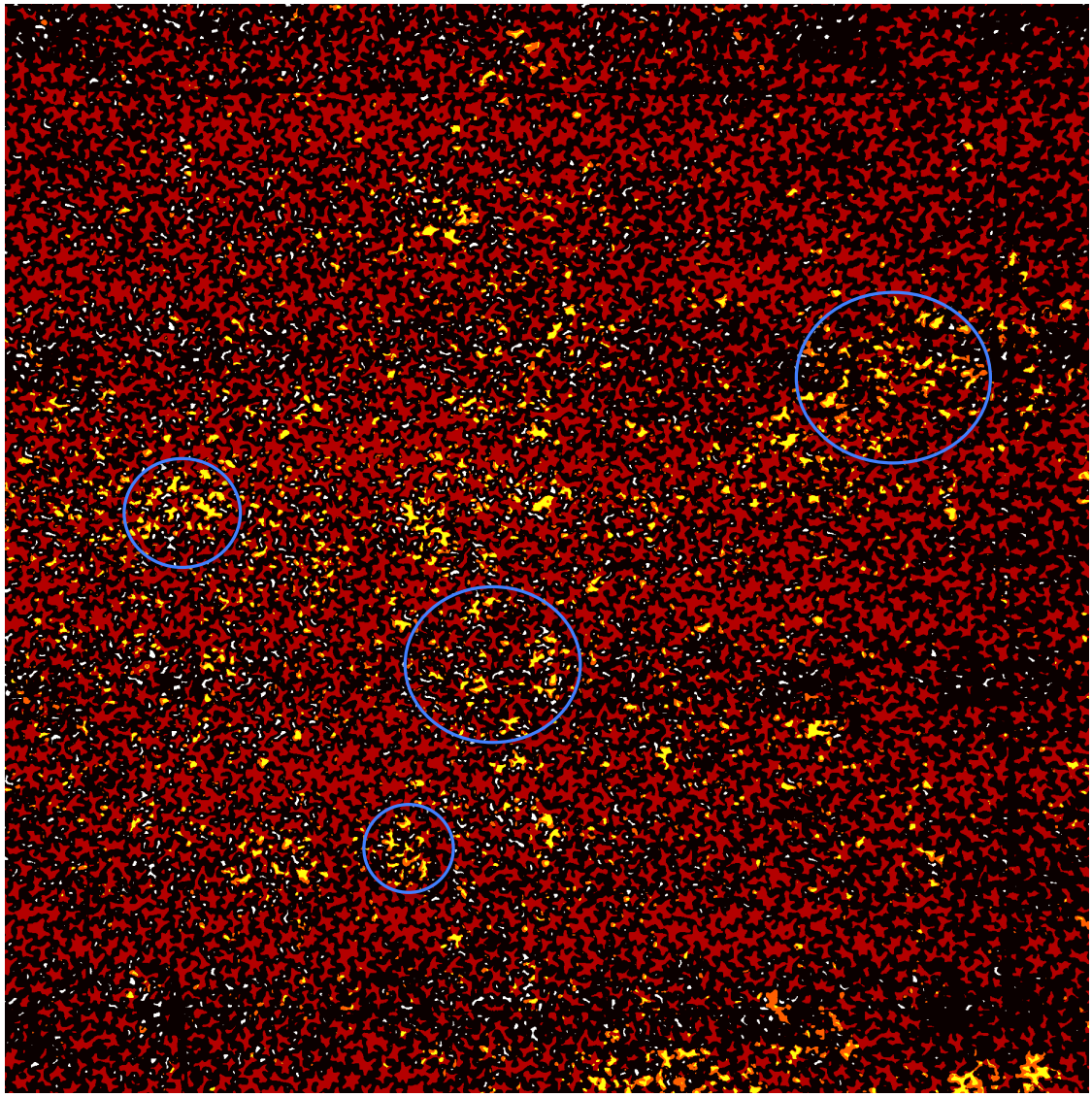

Figure 4.13: Overlaid image of high concentration of mobilized particles, with large aperture regions and straining dominant areas. The black and red regions are small and large apertures, respectively. The orange shows high concentration regions and yellow indicates where the high concentration of particles mobilized in large aperture. The white areas also represents regions with dominant straining.

4.4 Particle Retention and Effective Aperture

In order to better understand the relationship between accumulated particles and effective aperture, I tried to relate the measured effective apertures to the changes in aperture due to particle accumulation. By applying Equation 4.2, I calculated the concentration field over the entire fracture. This concentration can be translated to the volume of particles that are accumulated in each pixel. In our domain, for each pixel of the fracture there is one concentration and one associated aperture value. Therefore for each pixel we can write

$$V_{pixel} = ba \tag{4.5}$$

$$C = \frac{\rho_{kaolinite} V_{kaolinite}}{V_{water}} \tag{4.6}$$

$$V_{pixel} = V_{kaolinite} + V_{water} \tag{4.7}$$

where V is the volume b the aperture, a the area of the pixel and ρ the density of kaolinite. By rearranging these equations I can write

$$V_{kaolinite} = \frac{V_{pixel}}{\frac{\rho_{kaolinite}}{C} + 1} \tag{4.8}$$

This $V_{kaolinite}$ indicates the volume of particles; however we know that the actual volume occupied by the clay particles is larger than this value because of porosity of the settled particles. Therefore

$$V_{actual} = \frac{V_{kaolinite}}{n} \tag{4.9}$$

where n is the porosity of the settled particles and I assumed the value of 0.3 for it.

$$V_{pixel.new} = V_{pixel} - V_{actual} \tag{4.10}$$

By calculating the new volume for each pixel after subtracting the volume that is filled by the particles, I am able to estimate the new aperture value for each grid. It is expected that the new average of this aperture field to be close to the effective aperture that was calculated based on flow and head data. I performed this analyses for three different time during the experiment, after clay injection, after waterflooding and after oscillation. After clay injection Figure 4.6 shows the value of 10 μm for the effective aperture. By applying Equations 4.5 to 4.9, I found a new value of 64.72 μm for the new aperture which is far from the calculated value of 10 μm. Same analyses show the values of 69.81 and 71.12 μm for after flooding and after oscillation new apertures, respectively, which are closer to the calculated values of 58.77 and 73.23 μm but are not accurate. The hypothesis that I considered here is that effective aperture differs from mechanical aperture and by closing off some small apertures, we may decrease the effective aperture significantly while the mechanical aperture does not change that much. This was intuitive from Figure 4.13 where it is shown that during oscillation most of the particles were mobilized from regions surrounded by small aperture regions and that has significant effect on effective aperture value. To test this hypothesis, I ran a 2D simulation for flow field in the fracture. This simulation solves the differential flow equation for steady state condition in porous media. The equation is

$$T\frac{d^2h}{dx^2} + T\frac{d^2h}{dy^2} = 0 \tag{4.11}$$

where T is the transmissivity of the medium. Using Cubic law we can write for T

$$T = \frac{b^3 g}{12\nu} \tag{4.12}$$

To run this simulation using MATLAB, I converted the new calculated aperture field by above analyses, to transmissivity field and then calculated the flow field for 1 cm of H_2O head difference. Then the calculated flow rate and the 1 cm head were used in Cubic law to measure the effective aperture from them. The simulated effective aperture values were 64.43, 69.92 and 70.86 μm for after clay injection, after flooding and after oscillation, respectively which are close to the values calculated by above analyses.

Chapter 5

Summary and Conclusions

I conducted a set of experiments to examine effects of pore pressure oscillations on permeability of a fracture. The results showed that pore pressure oscillations will mobilize the particles and this particle mobilization enhances the permeability.

Here I present effective aperture as the representative value for the permeability of a fracture. I observed that for a fracture with effective aperture of 85.3 μm, particle retention due to gravitational sedimentation followed by a flushing process reduced effective aperture to 58.77 and pore pressure oscillations enhanced this value to 73.23 μm. I also visualized mobilization of the particles due to the oscillations. During the entire experiment images of fracture were taken by a camera. The animation produced with these images demonstrates the mobilization of the particles during the oscillation process. The animation is accessible through `https://www.youtube.com/watch?v=zwLmoRrncf0&feature=youtu.be`

In this study I manged to introduce a new suite of experiments to further analyze effects of pore pressure oscillations on fracture permeability. The direct relationship between oscillations and permeability enhancement was demonstrated and I successfully observed particle mobilization during oscillation. However further analyses needed to understand effects of

oscillations properties such as frequency and amplitude on the permeability enhancement and also better describe a relationship between the particle retention and effective aperture.

Bibliography

Maria Auset and Arturo A Keller. Pore-scale visualization of colloid straining and filtration in saturated porous media using micromodels. *Water resources research*, 42(12), 2006.

Jacob Bear. *Dynamics of fluids in porous media*. Courier Corporation, 2013.

Matthew W. Becker, Paul W. Reimus, and Peter Vilks. Transport and attenuation of carboxylate-modified latex microspheres in fractured rock laboratory and field tracer tests. *Ground Water*, 37(3):387–395, 1999. doi: 10.1111/j.1745-6584.1999.tb01116.x. URL `http://dx.doi.org/10.1111/j.1745-6584.1999.tb01116.x`.

Igor A Beresnev and Paul A Johnson. Elastic-wave stimulation of oil production: A review of methods and results. *Geophysics*, 59(6):1000–1017, 1994.

Emily E Brodsky, Evelyn Roeloffs, Douglas Woodcock, Ivan Gall, and Michael Manga. A mechanism for sustained groundwater pressure changes induced by distant earthquakes. *Journal of Geophysical Research: Solid Earth*, 108(B8), 2003.

Thibault Candela, Emily E Brodsky, Chris Marone, and Derek Elsworth. Laboratory evidence for particle mobilization as a mechanism for permeability enhancement via dynamic stressing. *Earth and Planetary Science Letters*, 392:279–291, 2014.

R Coble. The effects of the alaskan earthquake of march 27, 1964, on ground water in iowa. *Proc. Iowa Acad. Sci*, 72:323–332, 1965.

Russell L Detwiler, Scott E Pringle, and Robert J Glass. Measurement of fracture aperture fields using transmitted light: An evaluation of measurement errors and their influence on simulations of flow and transport through a single fracture. *Water resources research*, 35 (9):2605–2617, 1999.

Menachem Elimelech and Charles R. O'Melia. Kinetics of deposition of colloidal particles in porous media. *Environmental Science & Technology*, 24(10):1528–1536, 10 1990. doi: 10.1021/es00080a012. URL `http://dx.doi.org/10.1021/es00080a012`.

Jean E Elkhoury, Emily E Brodsky, and Duncan C Agnew. Seismic waves increase permeability. *Nature*, 441(7097):1135–1138, 2006.

Jean E Elkhoury, André Niemeijer, Emily E Brodsky, and Chris Marone. Laboratory observations of permeability enhancement by fluid pressure oscillation of in situ fractured rock. *Journal of Geophysical Research: Solid Earth*, 116(B2), 2011.

Igor Faoro, Derek Elsworth, and Chris Marone. Permeability evolution during dynamic stressing of dual permeability media. *Journal of Geophysical Research: Solid Earth*, 117 (B1):n/a–n/a, 2012. ISSN 2156-2202. doi: 10.1029/2011JB008635. URL http://dx.doi.org/10.1029/2011JB008635. B01310.

O.L. Kouznetsov, E.M. Simkin, G.V. Chilingar, and S.A. Katz. Improved oil recovery by application of vibro-energy to waterflooded sandstones. *Journal of Petroleum Science and Engineering*, 19(3–4):191 – 200, 1998. ISSN 0920-4105. doi: http://dx.doi.org/10.1016/S0920-4105(97)00022-3. URL http://www.sciencedirect.com/science/article/pii/S0920410597000223.

Weiqun Liu and Michael Manga. Changes in permeability caused by dynamic stresses in fractured sandstone. *Geophysical Research Letters*, 36(20):n/a–n/a, 2009. ISSN 1944-8007. doi: 10.1029/2009GL039852. URL http://dx.doi.org/10.1029/2009GL039852. L20307.

Paul F Luckham and Sylvia Rossi. The colloidal and rheological properties of bentonite suspensions. *Advances in Colloid and Interface Science*, 82(1–3):43 – 92, 1999. ISSN 0001-8686. doi: http://dx.doi.org/10.1016/S0001-8686(99)00005-6. URL http://www.sciencedirect.com/science/article/pii/S0001868699000056.

M. Manga and C.-Y. Wang. 4.10 - earthquake hydrology. In Gerald Schubert, editor, *Treatise on Geophysics*, pages 293 – 320. Elsevier, Amsterdam, 2007. ISBN 978-0-444-52748-6. doi: http://dx.doi.org/10.1016/B978-044452748-6.00074-2. URL http://www.sciencedirect.com/science/article/pii/B9780444527486000742.

Michael Manga. Did an earthquake trigger the may 2006 eruption of the lusi mud volcano? *Eos, Transactions American Geophysical Union*, 88(18):201–201, 2007. ISSN 2324-9250. doi: 10.1029/2007EO180009. URL http://dx.doi.org/10.1029/2007EO180009.

Michael Manga and Emily Brodsky. Seismic triggering of eruptions in the far field: Volcanoes and geysers. *Annual Review of Earth and Planetary Sciences*, 34(1):263–291, 2006. doi: 10.1146/annurev.earth.34.031405.125125. URL http://dx.doi.org/10.1146/annurev.earth.34.031405.125125.

MICHAEL Manga and JOEL C. Rowland. Response of alum rock springs to the october 30, 2007 alum rock earthquake and implications for the origin of increased discharge after earthquakes. *Geofluids*, 9(3):237–250, 2009. ISSN 1468-8123. doi: 10.1111/j.1468-8123.2009.00250.x. URL http://dx.doi.org/10.1111/j.1468-8123.2009.00250.x.

Michael Manga, Emily E. Brodsky, and Michael Boone. Response of streamflow to multiple earthquakes. *Geophysical Research Letters*, 30(5):n/a–n/a, 2003. ISSN 1944-8007. doi: 10.1029/2002GL016618. URL http://dx.doi.org/10.1029/2002GL016618. 1214.

Michael Manga, Igor Beresnev, Emily E. Brodsky, Jean E. Elkhoury, Derek Elsworth, S. E. Ingebritsen, David C. Mays, and Chi-Yuen Wang. Changes in permeability caused by

transient stresses: Field observations, experiments, and mechanisms. *Reviews of Geophysics*, 50(2):n/a–n/a, 2012. ISSN 1944-9208. doi: 10.1029/2011RG000382. URL http://dx.doi.org/10.1029/2011RG000382. RG2004.

Paul William Reimus. *The use of synthetic colloids in tracer transport experiments in saturated rock fractures*. PhD thesis, University of New Mexico Albuquerque, NM, 1995.

Evelyn A. Roeloffs. Persistent water level changes in a well near parkfield, california, due to local and distant earthquakes. *Journal of Geophysical Research: Solid Earth*, 103(B1): 869–889, 1998. ISSN 2156-2202. doi: 10.1029/97JB02335. URL http://dx.doi.org/10.1029/97JB02335.

Laurier L Schramm and Jan CT Kwak. Influence of exchangeable cation composition on the size and shape of montmorillonite particles in dilute suspension. *CLAYS CLAY MINER. Clays Clay Miner.*, 30(1):40, 1982.

Janusz Stawinski, Jacek Wierzchos, and María Teresa García González. Influence of calcium and sodium concentration on the microstructure of bentonite and kaolin. 1990.

Paul Adams Witherspoon, Joseph SY Wang, K Iwai, and John E Gale. Validity of cubic law for fluid flow in a deformable rock fracture. *Water resources research*, 16(6):1016–1024, 1980.

Lian Xue, Hai-Bing Li, Emily E. Brodsky, Zhi-Qing Xu, Yasuyuki Kano, Huan Wang, James J. Mori, Jia-Liang Si, Jun-Ling Pei, Wei Zhang, Guang Yang, Zhi-Ming Sun, and Yao Huang. Continuous permeability measurements record healing inside the wenchuan earthquake fault zone. *Science*, 340(6140):1555–1559, 2013. ISSN 0036-8075. doi: 10.1126/science.1237237. URL http://science.sciencemag.org/content/340/6140/1555.